PHARMACEUTICAL BIOLOGY
2026, VOL. 64, NO. 1, 312–333
https://doi.org/10.1080/13880209.2026.2629733

Taylor & Francis
Taylor & Francis Group

RESEARCH ARTICLE

OPEN ACCESS Check for updates

Phytochemical study of *Homalanthus giganteus*: isolation, antiproliferative activity, and computational mechanistic insights of tigliane diterpenes against colorectal cancer

Dyke Gita Wirasisya[a,b], Annamária Kincses[a], Arif Setiawansyah[c], Anita Barta[a], Fang-Rong Chang[d] and Judit Hohmann[a,e]

[a]Institute of Pharmacognosy, University of Szeged, Faculty of Pharmacy, Szeged, Hungary; [b]Department of Pharmacy, Faculty of Medicine, University of Mataram, Mataram, Indonesia; [c]Akademi Farmasi Cendikia Farma Husada, Bandar Lampung, Indonesia; [d]Graduate Institute of Natural Products, College of Pharmacy, Kaohsiung Medical University, Kaohsiung, Taiwan; [e]HUN-REN – USZ Biologically Active Natural Products Research Group, University of Szeged, Szeged, Hungary

ABSTRACT

Context: Colorectal cancer is the third most common and second deadliest cancer worldwide. Late diagnosis, poor outcomes in metastatic cases, and multidrug resistance emphasize the need for new therapies.

Objective: This study aimed to isolate bioactive compounds from *Homalanthus giganteus* Zoll. ex Miq. (Euphorbiaceae), evaluate their antiproliferative effects on colorectal cancer cells, and identify mechanisms through network pharmacology and molecular docking.

Materials and methods: Compounds were isolated by chromatographic separations, and the structures were elucidated by NMR and HRESIMS. The antiproliferative activity was measured by MTT assay. DFT calculations were performed in ORCA 6.1.0. Network pharmacology was used to identify targets and pathways, molecular docking with AutoDock Vina was used to determine binding affinities, and pkCSM was applied to predict pharmacokinetics and toxicity.

Results: 7β-Hydroxysitosterol (**1**), 7α-hydroxysitosterol (**2**), 12-*O*-palmitoyl-phorbol-13-acetate (**3**), 12-*O*-palmitoyl-7-oxo-5-ene-phorbol-13-acetate (**4**), cerevisterol (**5**), and β-sitosterol-3-*O*-glucoside (**6**) were isolated from *H. giganteus*. Compound **4** exhibited the highest activity against Colo 205 (IC_{50} 3.58 ± 0.37 µM) and Colo 320 cells (IC_{50} 6.06 ± 1.70 µM) and higher DFT stability. Network pharmacology and docking study revealed kinase-specific targeting (STAT3, JUN, PRKCA, GSK3β), with **4** preferentially binds PRKCA/GSK3β, whereas **3** favors STAT3/JUN. The pkCSM prediction server predicted good oral bioavailability, CYP3A4 metabolism, limited CNS penetration, and acceptable toxicity for both diterpenes.

Discussion and conclusions: Six compounds were isolated from *H. giganteus,* with **4** exhibiting antiproliferative activity through PRKCA and GSK3β modulation. These findings provide the first phytochemical and mechanistic evidence that support *H. giganteus* as a promising source of active anti-colon cancer leads.

ARTICLE HISTORY
Received 10 December 2025
Revised 5 February 2026
Accepted 6 February 2026

KEYWORDS
Homalanthus giganteus; Euphorbiaceae; tigliane diterpenoids; colorectal cancer; network pharmacology; molecular docking

Introduction

Colorectal cancer is the third most prevalent cancer worldwide and the second deadliest (Abedizadeh et al. 2024). The World Health Organization (WHO) predicted that the burden from colorectal cancer will increase by 63% (approximately 3.2 million cases) by 2040 (WHO 2023). Because its clinical manifestations appear at a late stage, many patients present with metastatic colorectal cancer with a survival rate below 12–15% (Siegel et al. 2023; Abedizadeh et al. 2024). Another major concern is the development of multidrug resistance, which involves alterations in drug metabolism, transportation, and the mutation of drug targets (Wang et al. 2022). Despite advances in immunotherapy and targeted chemotherapeutic treatment, colorectal cancer remains a global health concern, which underlies the urgent need for new therapies.

CONTACT Judit Hohmann hohmann.judit@szte.hu Eötvös Str. 6, 6720 Szeged, Hungary.
Supplemental data for this article can be accessed online at https://doi.org/10.1080/13880209.2026.2629733.

Natural products are invaluable sources of compounds with antitumor activity (Hashem et al. 2022; Naeem et al. 2022; Shaik et al. 2022). Over the last several decades, more than 140 anticancer drugs have been developed from natural compounds (Newman and Cragg 2020). The Euphorbiaceae family comprises over 6,300 species distributed across tropical and subtropical regions, except Antarctica. They have attracted considerable attention as a source for anticancer drug discovery because of their structurally diverse triterpenoid and diterpenoid content (Vasas and Hohmann 2014; Kemboi et al. 2021, 2020; Sánchez-Hoyos et al. 2024). Of these, tigliane, abietane, ingenane, and lathyrane-type diterpenes exert potent cytotoxic activity against various cancer cell lines (Hu et al. 2021; Alves et al. 2022; Vela et al. 2022; Ma et al. 2023; Otsuki and Li 2023; Zhou et al. 2025); however, their tumor-promoting properties have complicated clinical translation (Vogg et al. 1999; Baloch et al. 2005).

Homalanthus is a small genus from the Euphorbiaceae family. It comprises 23 species distributed throughout the Pacific (Wirasisya and Hohmann 2023). Despite its position within a chemically diverse family with ethnobotanically rich data, the genus remains underexplored with respect to the pharmacology of its phytochemicals. To date, only five species have been screened for pharmacological activity, and even fewer have undergone detailed phytochemical characterization. Previous studies of *H. populneus* and *H. nutans* revealed prostratin, a tigliane diterpene that garnered interest because of its HIV latency reversal activity (Gustafson et al. 1992; Johnson et al. 2008; Sintya et al. 2019). *H. nutans* is also known for its oxytocic activity and antibacterial activity against Gram-positive bacteria (Bourdy et al. 1996; Frankova et al. 2021), which highlights the therapeutic potential of compounds within this genus. The majority of *Homalanthus* species, including *H. giganteus*, have not received significant attention despite their established ethnobotanical use in Indonesia and other parts of Southeast Asia and the Pacific (Wirasisya and Hohmann 2023).

Our preliminary screening of Euphorbiaceae revealed that *H. giganteus* crude extracts exhibit marked antiproliferative effects against human colon cancer cell lines (Wirasisya et al. 2023). These initial results prompted us to perform a phytochemical investigation to identify the components responsible for this activity. The antiproliferative activity of several isolated compounds was evaluated against doxorubicin-sensitive (Colo 205) and doxorubicin-resistant (Colo 320) human colorectal cancer cell lines. We also examined how their structures were related to their effectiveness. Computer-based methods were used to determine how these diterpenes interact with colorectal cancer cells at the molecular level.

Experimental methods

General experimental procedures

Nuclear magnetic resonance (NMR) spectra were generated on Bruker Ascend 500 (500 MHz for ^{1}H, 125 MHz for ^{13}C), except for the 2D NMR spectra of **3** and **4** which were measured on Bruker AVANCE III 600 (600 MHz for ^{1}H, 150 MHz for ^{13}C) spectrometers (Bruker BioSpin, Germany). High-resolution electrospray ionization mass spectrometry (HRESIMS) was carried out on a Thermo Scientific Q Exactive Plus Orbitrap mass spectrometer (Thermo Fisher Scientific, USA), which was operated in positive or negative ionization mode. Centrifugal partition chromatography (CPC) was conducted on a pilot-scale (RPCC) (Rotachrom Technologies, Budapest, Hungary). Open column chromatography (OCC) was performed using silica gel 60 (0.045–0.063 mm; Molar Chemicals, Budapest, Hungary, Product No. CM0098429), polyamide (50–160 µm; MP Biomedicals, Irvine, USA, Product No. 0209602), and Sephadex LH-20 (25–100 µm bead size; Cytiva, Uppsala, Sweden, Product No. 17-0090-01) columns. Vacuum liquid chromatography (VLC) silica gel 60 (15–40 µm; Molar Chemicals, Budapest, Hungary, Product No. BX3394455 was used. Flash chromatography (FC) was done using a CombiFlash NextGen 300+ system (Teledyne ISCO, Lincoln, NE, USA) equipped with dual-wavelength UV (254/280 nm) and a photodiode array (PDA), using RediSep Rf Gold High-Performance silica columns (12 g; Teledyne ISCO, Product No. 69-2203-345). Rotary planar chromatography (RPC, Chromatotron) was performed on a Harrison Research Model 7924 T instrument (Harrison Research, Palo Alto, CA, USA) with silica gel 60 GF_{254} (Merck, Darmstadt, Germany, Product No. 1.07749.1000). Thin-layer chromatography (TLC) was carried out using precoated silica gel 60 F_{254} aluminum sheets

(20 × 20 cm, 0.2 mm layer thickness; Merck, Product No. 1.05554.0001). The compounds were visualized under UV light (254 and 365 nm) and after spraying with concentrated sulfuric acid (cc. H_2SO_4) and heating at 105 °C for 3–5 min. For semipreparative and analytical high-performance liquid chromatography (HPLC), a Shimadzu LC-2010CHT system (Shimadzu, Kyoto, Japan) equipped with a UV-Vis detector was used. Semipreparative separations were achieved using a Phenomenex Kinetex C_{18} column (100 Å pore size, 5 µm particle size, 250 × 10 mm; Phenomenex, CA, USA, Product No.00G-4601-E0). For analytical separation, a Phenomenex Luna C_8 column (100 Å, 5 µm, 250 × 4.6 mm, Phenomenex, CA, USA, Product No. 00 G-4249-EO) was used. Analytical grade solvents were supplied by Molar Chemicals Kft. (Halásztelek, Hungary): methanol (Product No. 05730-006-410), *n*-hexane (Product No. 06850-101-411), *n*-heptane (Product No. 06830-101-350), CH_2Cl_2 (Product No. 02592-101-350), ethyl acetate (Product No. 02930-101-411). Solvents for HPLC were purchased from VWR International Kft. (Debrecen, Hungary): cyclohexane (Product No. 83629.320), and methanol (Product No. 20864.320). The water was supplied by the Milli-Q Direct 3 UV pump (Merck, Darmstadt, Germany).

Plant materials

Fresh *Homalanthus giganteus* Zoll. ex Miq. (Euphorbiaceae) leaves were collected in June 2022 from Lombok Island, West Nusa Tenggara Province, Indonesia. The plant was collected and authenticated by Dr. I Gde Mertha, a taxonomist in the Department of Biology Education, Faculty of Teacher Training and Education, University of Mataram, Indonesia, through a comparison with herbarium specimens and morphological markers. A voucher specimen (collection number DGW-03) was deposited at the Herbarium in the Department of Forestry, Faculty of Agriculture, University of Mataram, Mataram, Indonesia.

Extraction and isolation

Freshly collected leaves were oven-dried, which resulted in 2.98 kg of dried leaves. They were ground into a powder and extracted by percolation with methanol (120 L) at room temperature. The combined extracts were concentrated under reduced pressure using a rotary evaporator to yield a crude MeOH extract (586.5 g, 19.7% yield based on dry weight). The crude extract (586.5 g) was partitioned with an *n*-heptane/ethyl acetate upper phase and subsequently filtered through a 10-µm paper filter to yield an insoluble (432.9 g, 73.8%) and a soluble (153.6 g, 26.2%) fraction. The soluble fraction (153.6 g) was subjected to CPC in a descending mode (elution–extrusion, 30–30 min), using a solvent system consisting of *n*-heptane/ethyl acetate/methanol/water (1:1:1:1, v/v) at a flow rate of 200 mL/min and a speed of 1,000 rpm for 27 min. The separation yielded four fractions, which were pooled into four main fractions (HG1–HG4).

Fraction HG4 (82.7 g) was separated by polyamide OCC with a stepwise gradient of MeOH/H_2O (40:60; 60:40; 80:20; 100:0, v/v, 450 mL each mixture). They were pooled to yield four subfractions (HG4.A–D). Subfraction HG4.C (10.29 g) was similarly fractionated by VLC using cyclohexane/EtOAc/MeOH (100:0:0, 98:2:0, 95:5:0, 90:10:0, 80:20:0, 50:45:5, 40:50:10, and 30:50:20, v/v, 250 mL each mixture) to yield 16 subfractions (HG4.C1–C16).

Subfraction HG4.C10 (284.5 mg) was subjected to silica gel OCC with a gradient of *n*-hexane/EtOAc/MeOH (100:0:0, 90:10:0, 75:25:0, 60:40:0, 50:50:0, 35:35:20, and 0:0:100, v/v) using 100 mL each mixture except the final eluent (200 mL) to yield six subfractions (HG4.C10a–f). Subfraction HG4.C10c (157.6 mg) was purified by Sephadex LH-20 OCC and eluted with mixtures of MeOH/CH_2Cl_2 (1:1, v/v, 215 mL) to obtain two subfractions (HG4.C10c1–2). Subfraction HG4.C10c2 (49.9 mg) was subjected to silica gel OCC using *n*-hexane/EtOAc (9:1, 8:2, 7:3, and 6:4, v/v, 100 mL each mixture), which yielded 12 fractions (HG4.C10c2.I–XII). Final purification of HG4.C10c2.X (8.6 mg) was done by semipreparative RP-HPLC (Phenomenex Luna C_8, 250 × 10 mm; MeOH/H_2O 95:5, v/v; flow rate 2.0 mL/min) to yield compounds **1** (0.52 mg, *t*R: 17 min) and **2** (0.57 mg, *t*R: 19 min).

HG4.C11 (675.0 mg) was fractionated by RPC using a gradient system of CH_2Cl_2/MeOH (100:0, 99:1, 98:2, 97:3, 96:4, 95:5, and 90:10, v/v, 100 mL each mixture). This separation was performed in

six sequential runs used approximately 110 mg of fraction per runs. Fractions were combined based on TLC monitoring, which afforded 11 subfractions (HG4.C11a–k). Subfraction HG4.C11c (46.6 mg) was separated by semipreparative RP-HPLC (Phenomenex Kinetex C_{18}, MeOH/H_2O 90.5:9.5, v/v; flow rate 0.5 mL/min), resulting in compound **3** (2.8 mg, *t*R 28 min). The remaining material from HG4.C11c (12.3 mg) was further purified by analytical HPLC (Phenomenex Kinetex C_{18}, MeOH/H_2O 89:11, v/v; flow rate 0.7 mL/min) to yield compound **4** (1.2 mg, *t*R 14 min). Compound **5** (1 mg, t_R = 18) was isolated from fraction HG4.C11h3 (15.05 mg) by semipreparative reversed-phase HPLC using isocratic system of MeOH/H_2O (87:13, flow rate of 0.7 mL/min).

Subfraction HG4.C12 (749.2 mg) was separated by FC (RediSep Rf Gold 12 g silica column) using a gradient of CH_2Cl_2/MeOH (99:1, 97:3, 95:5, 90:10, and 0:100, v/v, flow rate 17 mL/min) over 75 min to yield 14 subfractions (HG4.C12a–n). Subfraction HG4.C12i (257.8 mg) was subjected to silica gel VLC with a gradient system of CH_2Cl_2/MeOH (99:1, 97:3, 96:4, 95:5, 90:10, and 0:100, v/v) using 100 mL each mixture except the final eluent (200 mL), affording seven subfractions (HG4.C12i1–7). Final purification of HG4.C12i6 (119.6 mg) by RPC was done on a silica gel using gradient elution with CH_2Cl_2/MeOH (100:0, 99:1, 97:3, 95:5, 94:6, 90:10, and 0:100, v/v, 100 mL each mixture), which resulted in compound **6** (12.3 mg).

Cell lines

The human colon adenocarcinoma cells, Colo 205 (Product Code ATCC-CCL-222, doxorubicin-sensitive, CVCL_0218) and Colo 320/MDR-LRP (Product Code: ATCC- CCL-220.1, multidrug-resistant, expressing P-gp, CVCL_0220), were sourced from LGC Promochem (Teddington, England). The cell lines were cultured in RPMI 1640 medium containing 10% heat-inactivated fetal bovine serum, 2 mM L-glutamine, 1 mM sodium pyruvate, and 100 mM HEPES (Merck, Darmstadt, Germany, Product No. R8758-6X500ML). The cells were incubated at 37 °C in a 5% CO_2 and 95% air atmosphere.

Antiproliferative assay

Human colon adenocarcinoma cell lines, Colo 205 and Colo 320, were employed to investigate the impact of the test compounds on cell proliferation. Experiments were carried out in 96-well flat-bottomed microtiter plates. Stock solutions of the compounds were prepared in dimethyl sulfoxide (DMSO, Molar Chemicals Kft., Product No. 02610-526-340), ensuring that the final DMSO concentration in the wells did not exceed 1%. Compounds were diluted in 100 µL of RPMI medium, and 6×10^3 cells suspended in 100 µL of RPMI medium were added into each well, except for the medium control wells. Plates were incubated at 37 °C for 72 h, after which 20 µL of a 5 mg/mL MTT (thiazolyl blue tetrazolium bromide) solution (Merck, Darmstadt, Germany, Product No. M5655) was added to each well. Following a 4-h incubation at 37 °C, 100 µL of 10% sodium dodecyl sulfate (Merck, Darmstadt, Germany, Product No. 71736) in 0.01 M HCl (Molar Chemicals Kft., Halásztelek, Hungary, Product No. 08710) was added to dissolve the formazan crystals, and the plates were left overnight at 37 °C. Cell viability was assessed by measuring the optical density at 540/630 nm using a Multiscan EX ELISA reader (Thermo Labsystems, Cheshire, WA, USA). Cell viability was expressed as a percentage of untreated control cells, which were defined as 100%. Doxorubicin (Sandoz, Basel, Switzerland, Product No. 107209) served as the positive control. Cells treated with 1% DMSO without test compounds served as the solvent control. The concentration of each compound that reduced cell viability by 50% (IC_{50}, µM) was calculated using GraphPad Prism version 5.00 for Windows, employing non-linear regression analysis of dose-response curves (GraphPad Software Inc., San Diego, CA, USA). IC_{50} values were derived from four independent experiments for each cell line and are presented as mean values (Barta et al. 2025).

DFT calculation

Quantum chemical calculations were conducted using ORCA version 6.1.0 software (Neese 2025) and Avogadro 1.2.0 was used to visualize the results. The computational process began with geometry optimization based on density functional theory methods, and applying the B3LYP function with def2-SVP basis set parameters and def2/J functions. Frequency calculations were performed using the

same theoretical approach to confirm that the optimized structure corresponded to a true minimum energy configuration. Electronic properties and physicochemical characteristics were examined through frontier molecular orbital analysis and molecular electrostatic potential mapping at the B3LYP/def2-SVP and def2/J theoretical level. This computational approach included a global chemical reactivity descriptor analysis to provide comprehensive information regarding the molecular stability of the studied compound. These global chemical reactivity descriptors were calculated using the method described by Abu-Izneid et al. (2024):

Energy gap:

$$E\_gap = \mathrm{E}_{\mathrm{LUMO}} - \mathrm{E}_{\mathrm{HOMO}} \tag{1}$$

Electron affinity:

$$A = -\mathrm{E}_{\mathrm{LUMO}} \tag{2}$$

Electron ionization:

$$I = -\mathrm{E}_{\mathrm{HOMO}} \tag{3}$$

Chemical hardness:

$$\eta = \frac{I - A}{2} \tag{4}$$

Chemical softness:

$$S = \frac{1}{2\eta} \tag{5}$$

Electronegativity:

$$\chi = \frac{I + A}{2} \tag{6}$$

Chemical potential:

$$\mu = -\left(\frac{I + A}{2}\right) \tag{7}$$

Electrophilicity index:

$$\omega = \frac{\mu^2}{2\eta} \tag{8}$$

Network pharmacology

A targeted-network pharmacology study was carried out based on a previously described method (Sadaqa et al. 2025; Susanti et al. 2025). Canonical SMILES of all compounds were submitted to Swiss Target Prediction (https://www.swisstargetprediction.ch). The predicted gene targets were validated and standardized using UniProt (https://www.uniprot.org), then intersected with colon cancer-associated genes from GeneCards (https://www.genecards.org) using Venny 2.1.0 (https://bioinfogp.cnb.csic.es/tools/venny/). Protein–protein interaction networks were generated using the STRING database (https://string-db.org) and visualized with Cytoscape 3.10.1 for topological analysis. Hub targets were identified based on pathway enrichment and biological process analysis through STRING with a false discovery rate threshold of <0.05.

Molecular docking

Molecular docking was conducted using AutoDock Vina (Trott and Olson 2010) to evaluate compound–target interactions. The diterpene structures were drawn in ChemDraw Professional and energy-minimized in Avogadro using the MMFF96 force field with the steepest descent algorithm. Crystal structures of STAT3 (PDB: 6NUQ), JUN (PDB: 4Y46), PRKCA (PDB: 8U73), and GSK3β (PDB: 7OY6) were retrieved from the RCSB Protein Data Bank and prepared by removing water molecules, heteroatoms, and non-essential chains using BIOVIA Discovery Studio Visualizer 2021. Ligands were energy-minimized *via* OpenBabel using UFF force field with steepest descent algorithm (500 steps with an energy gradient threshold of 1.0×10^{-6} kcal/mol) and converted to PDBQT format. Docking simulations utilized a grid spacing of 0.375 Å with an exhaustiveness of 32, and were optimized to encompass binding site residues (Susianti et al. 2024). Five replicates were performed per simulation, with the lowest energy conformation analyzed for the binding interactions using BIOVIA Discovery Studio Visualizer.

Pharmacokinetics and toxicology prediction

The pharmacokinetic properties and toxicity profiles of the two diterpene compounds were evaluated by computational methods using the pkCSM prediction server (https://biosig.lab.uq.edu.au/pkcsm). The evaluation process involved submitting the canonical SMILES notation for each molecule into the designated SMILES string field within the pkCSM web interface (Pires et al. 2015).

Results

Isolated compounds

Fractionation of the MeOH extract of *H. giganteus* leaves, followed by extensive chromatographic purification, as detailed in experimental section, yielded the following six compounds: 7β-hydroxysitosterol (**1**) (Chaurasia and Wichtl 1987), 7α-hydroxysitosterol (**2**) (Chaurasia and Wichtl 1987), 12-*O*-palmitoyl-phorbol-13-acetate (**3**) (Ohigashi et al. 1983; Pei et al. 2012), 12-*O*-palmitoyl-7-oxo-5-ene-phorbol-13-acetate (**4**) (Ohigashi et al. 1983), cerevisterol (**5**) (Zhao et al. 2010) and β-sitosterol-3-*O*-β-D-glucoside (**6**) (Peshin and Kar 2017). All compounds from *H. giganteus* are reported here for the first time. Structural determination was carried out through a comprehensive spectroscopic analysis, including 1D and 2D NMR (^{1}H and ^{13}C) and HRESIMS supplemented by comparison with the literature data (Figure 1).

Compounds **1** and **2** were obtained as white amorphous powders. Both compounds appeared as intense royal blue spots by TLC after spraying with sulfuric acid reagent and heating at 105 °C. This chromogenic response is characteristic of 7-oxygenated sterols (Chicoye et al. 1968). The structures were identified from ^{1}H,^{13}C NMR, HSQC, HMBC, and NOESY spectra. For both compounds, the 7-hydroxy-β-sitosterol structure was elucidated. The difference was in the stereochemistry of C-7, which was established by NOESY. Correlations between the H-7 and H-15α indicated a β orientation of the hydroxyl group for **1**, and the correlation between H-7 and H-8, and H-7 and H-15β indicated a position for **2**. Our NMR data were consistent with those published by Chaurasia and Wichtl (1987) for 7β-hydroxy-β-sitosterol (**1**) and 7α-hydroxy-β-sitosterol (**2**). Our NMR results enabled us to determine NMR data in other solvents previously reported and provided the full ^{1}H NMR assignments for the first time. The ^{13}C NMR (CD_3OD, 125 MHz) of compound **1** yielded 29 carbon signals, including signals for a trisubstituted olefin group (δ_C 144.1, C-5; δ_C 127.4 C-6), which corresponded to a 7-hydroxysitosterol structure.

Compounds **3** and **4** were isolated as a colorless oil. The molecular formula of compound **3** was established by HRESIMS neg *m/z* 643.4232 $[M - H]^-$ (calcd for $C_{38}H_{59}O_8^-$, 643.4215) and HRESIMS pos *m/z* 627.4252 $[M + H - H_2O]^+$ (calcd for $C_{38}H_{59}O_7^+$, 627.4256), which indicated nine degrees of unsaturation.

The ^{1}H NMR spectra of compound **3** showed six methyl signals at δ_H 0.89 (1H, d, J = 6.8 Hz, H-18), 0.90 (1H, t, J = 6.6 Hz, H-16′), 1.22 (1H, s, H-17), 1.26 (1H, s, H-16), 1.74 (1H, d, J = 1.7 Hz,

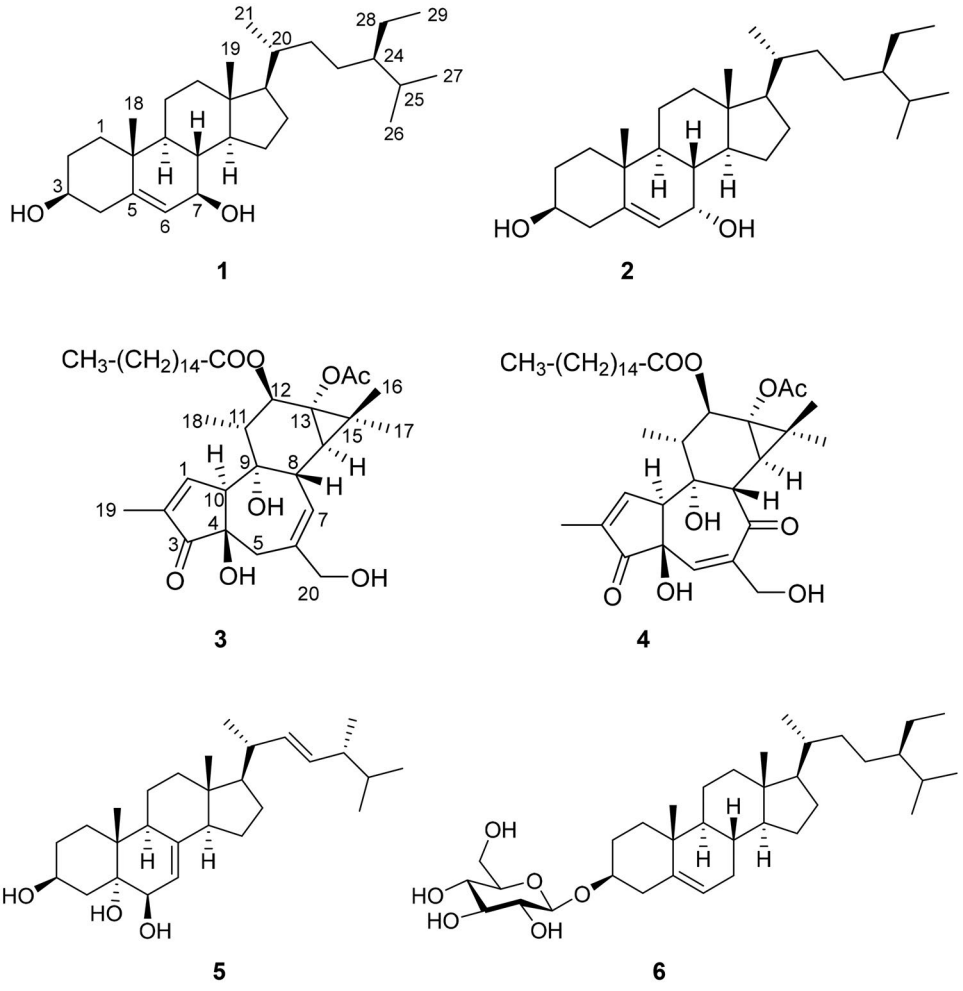

Figure 1. Structure of compounds **1**–**6**.

H-19), and 2.06 (1H, s, H-2′′), along with two methine signals at δ_H 3.29 (1H, m, H-8) and 3.16 (1H, t, J = 2.5 Hz, H-10). Three olefinic signals were also observed at δ_H 7.55 (1H, s, H-1), 5.62 (1H, d, J = 5.3 Hz, H-7), and 5.45 (1H, d, J = 10.5 Hz, H-12) (Table 1). The ^{13}C NMR spectra revealed the presence of one ketone carbonyl at δ_C 210.3 (C-3), four olefinic carbons at δ_C 160.5 (C-1), 134.6 (C-2), 142.9 (C-6), and 129.3 (C-7), along with two ester carbonyl carbons at δ_C 175.7 (C-1′) and 175.3 (C-1′′). The spectroscopic features, including one ketone carbonyl and four olefinic carbons, are characteristic of a tigliane-type diterpenoid skeleton (Wu et al. 2009; Forgo et al. 2011; Krstić et al. 2025). The two ester carbonyl signals indicated esterification at C-12 and C-13, which is typical for this class of compounds (Wu et al. 2009; Appendino and Gaeta 2024). A detailed analysis of the NMR data combined with the HRESIMS peaks confirmed the presence of an acetyl group and a hexadecanoyl (palmitic acid) moiety as ester substituents. Comparison of the spectroscopic data with the literature revealed compound **3** as 12-*O*-palmitoyl-phorbol-13-acetate, which was previously isolated from *Aleurites fordii* and *Sapium sebiferum* (Ohigashi et al. 1983; Pei et al. 2012).

The molecular formula of compound **4** was also established by HRESIMS pos *m/z* 681.3963 $[M+Na]^+$ (calcd for $C_{38}H_{58}O_9Na^+$, 681.3974), which indicated 10 degrees of unsaturation. The ^{1}H NMR spectrum (CD_3OD, 500 MHz) displayed signals for two olefinic protons at δ_H 7.60 (1H, s, H-1) and 6.95 (1H, s, H-5), along with six methyl groups at δ_H 1.22 (1H, s, H-16), 1.19 (1H, s, H-17), 0.94 (1H, d, J = 6.5 Hz, H-18), 1.81 (1H, s, H-19), 0.90 (1H, t, J = 6.6 Hz, H-16′), and 2.09 (1H, s, H-2′′), and two methine groups at δ_H 3.82 (1H, d, J = 5.6 Hz, H-8) and 3.11 (1H, t, J = 2.6 Hz, H-10).

The ^{13}C NMR (CD_3OD, 125 MHz) spectra showed two ketone carbonyls at δ_C 206.1 (C-3) and 200.1 (C-7). Three olefinic carbons were observed at δ_C 134.9 (C-2), 138.3 (C-5), and 149.5 (C-6), with two ester carbonyl carbons at δ_C 173.2 (C-1′) and 175.6 (C-1′′). The ^{1}H and ^{13}C NMR data for

Table 1. NMR data for compounds **3** and **4** [CD_3OD, 500 MHz (^1H), 125 MHz (^{13}C), δ ppm, J = Hz].

	3		**4**	
Position	^1H NMR	^{13}C NMR	^1H NMR	^{13}C NMR
1	7.55 s	160.5	7.60 s	nd
2	–	134.6	–	136.9
3	–	210.3	–	206.1
4	–	74.3	–	nd
5	2.48 d (18.9) 2.54 d (18.9)	38.5	6.95 s	138.3
6	–	142.9	–	149.5
7	5.62 d (5.3)	129.3	–	200.1
8	3.29 m	40.0	3.82 d (5.6)	55.7
9	–	79.8	–	77.4
10	3.16 t (2.5)	57.3	3.11 t (2.6)	60.3
11	2.22 m	44.3	2.30 dd (10.4, 6.5)	45.8
12	5.45 d (10.5)	78.2	5.46 d (10.4)	77.7
13	–	67.1	–	67.2
14	1.16 d (5.3)	37.1	1.80 d (5.6)	30.8
15	–	27.2	–	26.8
16	1.26 s	17.4	1.22 s	17.3
17	1.22 s	24.1	1.19 s	23.7
18	0.89 d (6.8)	14.4	0.94 d (6.5)	14.8
19	1.74 d (1.7)	10.2	1.81 s	10.4
20	3.92 d (13.0) 3.96 d (13.0)	68.0	4.25 s (2H)	62.4
12-palmitoyl				
1′	–	175.7	–	173.2
2′	2.35 m (2H)	35.4	2.36 m	35.3
3′	1.64 m (2H)	26.3	1.64 m	26.3
4′-15′	1.28 – 1.35 m	23.7 – 30.8	1.28 – 1.35 m	23.8 – 30.8
16′	0.90 t (6.6)	14.8	0.90 t (6.6)	14.4
13-Acetyl				
1″	–	175.3	–	175.6
2″	2.06 s	21.0	2.09 s	21.0

nd = not detected.

compound **4** (Table 1) revealed a close similarity to compound **3**, with the addition of one ketone group. Comparison of the spectroscopic data with the literature values indicated that compound **4** is 12-*O*-palmitoyl-7-oxo-5-ene-phorbol-13-acetate, which was previously isolated from *Sapium sebifereum* (Ohigashi et al. 1983). Table 1 contains NMR data for **3** and **4**, which were previously unpublished in a CD_3OD solvent.

Compound **5** was isolated as a white powder. 1D and 2D NMR indicated a C_{28} sterol. Its structure was determined by comparison with literature data, as cerevisterol (Zhao et al. 2010). Compound **6** was isolated as a white powder. Its NMR data were consistent with the published data of Peshin and Kar (2017) and was identified as β-sitosterol-3-*O*-β-D-glucoside.

Antiproliferative activity

The phytochemical investigation of *H. giganteus* leaves was motivated by our previous studies that revealed promising bioactivities of the non-polar fraction against colon cancer cells Colo 205 and Colo 320 (Wirasisya et al. 2023). Accordingly, the isolated compounds were tested against these cell lines for antiproliferative activity. The results are presented in Table 2. Relative resistance factors (RF) were also calculated, which represent how much more resistant the Colo 320 cell line is to the chemotherapeutic treatment compared to Colo 205.

Based on this study, the diterpenes (**3** and **4**) were the most effective compounds, followed by triterpenes (**1**, **2,** and **6**) against Colo 205 and Colo 320 cell lines. This is consistent with the extensive literature on Euphorbiaceae constituents, in which the diterpenes typically show superior activity compared with the triterpenes (Kemboi et al. 2021; Jiménez-González et al. 2023; Shakeri et al. 2024).

Despite their close structural resemblance and differing only in the stereochemistry of the C-7 hydroxyl group, compounds **1** and **2** showed a difference in activity. The 7β-hydroxysitosterol (**1**) was 3.8- and 1.8-fold more potent compared with that of 7α-hydroxysitosterol (**2**) against Colo 205 and Colo 320 cells, respectively. Interestingly, **2** was more effective against the drug-resistant cell line

compared with the sensitive cell line (RF = 0.68). The preference for the β-configuration in cytotoxic activity is consistent with earlier findings on oxysterols (Roh et al. 2010). Roussi et al. (2007, 2005) reported the superior activity of compound **1**, which induced apoptosis in Caco-2 colon cancer cells through the sequential activation of caspase-9 and caspase-3, coupled with DNA fragmentation and mitochondrial membrane permeabilization.

In the antiproliferative assay, compound **4** showed 3.5- and 5.0-fold enhanced potency compared with compound **3** against Colo 205 and Colo 320 cells, respectively. Structurally, compound **3** contains a $\Delta^{6(7)}$ double bond, whereas compound **4** has a $\Delta^{5(6)}$ double bond and a 7-ketone. The presence of the $\Delta^{6(7)}$ double bond in tigliane diterpenes facilitates oxidative rearrangements (Appendino and Gaeta 2024). Both compounds have been isolated from *Sapium sebiferum* (Ohigashi et al. 1983). Compound **3** was originally isolated from *Aleurites fordii* seeds and found to have immunomodulatory activity (IFN-γ induction in NK92 cells) (Pei et al. 2012); however, it did not exert cytotoxicity against SNU387 hepatoma cells (Zhang et al. 2013).

Compounds **3** and **4** are tigliane esters, a class known for their tumor-promoting activity through sustained protein kinase C (PKC) activation (Vasas and Hohmann 2014). They also induce Epstein-Barr virus early antigen (EBV-EA) activation, a marker of tumor promotion (Ohigashi et al. 1983). In addition, compound **3** exhibits piscicide activity comparable with rotenone (Hirota et al. 1979), indicating acute toxicity. Therefore, comprehensive toxicity profiling is essential before considering further development.

Compound **6** (β-sitosterol-3-*O*-glucoside), also known as daucosterol, is a ubiquitous plant sterol glycoside with known anticancer activity. Previous studies reported the low potency of **6** against colon cancer, which was consistent with our results. Wang et al. reported IC_{50} values of 26.6 µM and 47.3 µM in HCT-116 colon cancer cells at 24 and 48 h, respectively, accompanied by sub-G_1 cell cycle arrest (Wang et al. 2016). Compound **6** showed an RF value of 0.45, which suggests a drug resistance-modifying activity and collateral sensitivity effects (Hall et al. 2009).

As a positive control, doxorubicin exhibited IC_{50} values of 0.36 ± 0.12 µM (Colo 205) and 1.72 ± 0.50 µM (Colo 320), with a resistance factor (RF) of 4.8, which confirms the multidrug-resistant phenotype of Colo 320 cells. Of the isolated compounds tested, **4** showed the most potent activity with IC_{50} values of 3.58 ± 0.37 µM (Colo 205) and 6.06 ± 1.70 µM (Colo 320); however, compound **4** only had a moderate RF of 1.7 compared with doxorubicin (RF = 4.8). Compound **3** exhibited moderate activity with IC_{50} values of 12.37 ± 0.44 µM (Colo 205) and 30.36 ± 4.37 µM (Colo 320), but showed a slightly higher tumor cell selectivity (RF of 2.5).

DFT calculation

To elucidate the differences in antiproliferative potency between compounds **3** and **4**, density functional theory (DFT) calculations were conducted. DFT analysis revealed intrinsic electronic properties that affect molecular reactivity, selectivity, and stability for compounds **3** and **4** (Rong et al. 2020).

The HOMO-LUMO energy gap was 4.756 eV for compound **3** (Figure 2(A)) and 5.236 eV for compound **4** (Figure 2(B)), with a difference of approximately 0.48 eV. Because smaller energy gaps are generally associated with increased molecular polarizability and higher chemical reactivity (Miar et al. 2021; Casares et al. 2022), compound **3** appeared more susceptible to electrophilic and nucleophilic attack. For compound **3**, HOMO electron density was concentrated around the hydroxyl-bearing cyclopentane and oxygen functionalities, indicating a nucleophilic center, whereas LUMO distribution

Table 2. Antiproliferative activities of the isolated compounds against colorectal cancer cell lines.

Compound	IC_{50} (µM) Colo 205	IC_{50} (µM) Colo 320	RF*
1	22.20 ± 2.06	31.31 ± 3.10	1.41
2	83.52 ± 5.55	57.61 ± 4.80	0.68
3	12.37 ± 0.44	30.36 ± 4.37	2.45
4	3.58 ± 0.37	6.06 ± 1.70	1.69
6	>100	45.15 ± 2.38	0.45
Doxorubicin	0.36 ± 0.12	1.72 ± 0.50	4.77

*Relative resistance factor: IC_{50}(Colo 320)/IC_{50}(Colo 205).

indicated potential electrophilic sites. The larger energy gap in compound **4** reflects enhanced kinetic stability (Miar et al. 2021), which was likely the result of acetylation and oxidation at C-7, which withdraws electron density and stabilizes the molecular orbitals. This computational finding validates previous results showing the presence of the $\Delta^{6(7)}$ double bond in tigliane diterpenes, which renders the compound more reactive and triggers rearrangements (Appendino and Gaeta 2024).

Molecular electrostatic potential (MEP) maps revealed the charge distribution across both molecules. For compound **3** (Figure 2(C)), electron-rich regions (red) were localized around the oxygen atoms of hydroxyl and carbonyl groups, which is consistent with a nucleophilic character. Electron-poor regions (blue) appeared near the hydrogens bound to electronegative atoms, which are potential sites for electrophilic attack or hydrogen bonding. Compound **4** displayed an altered electrostatic distribution because of the C-13 acetyl group and C-7 ketone, which created distinct electrostatic environments that may influence target protein interactions (Figure 2(D)).

Global chemical reactivity descriptors were used to quantify these differences (Table 3). The HOMO energies for the compounds were −6.671 eV (**3**) and −6.698 eV (**4**), with LUMO energies at −1.915 eV and −1.462 eV, respectively. Electron affinity decreased from 1.915 eV (compound **3**) to 1.462 eV (compound **4**), which indicated reduced electron-accepting capacity following structural modification. Ionization potential increased slightly from 6.671 to 6.698 eV. Based on these results, a lower electron affinity was associated with a decreased ability to undergo reduction, and higher ionization potential signals increased molecular stability toward oxidation, which suggests that compound **4** binds electrons more tightly (Radhi 2020; Miar et al. 2021).

Chemical hardness (η) was higher for compound **4** (2.618 eV vs. 2.378 eV), thus confirming it as the "harder", less polarizable system. Chemical softness (S) was greater for compound **3** (0.210 vs. 0.191 eV^{-1}), which indicates its higher polarizability and greater chemical reactivity (Abbaz et al. 2018; Kaya and Putz 2022). Electronegativity (χ) remained similar at 4.293 eV for compound **3** and 4.080 eV for compound **4**. This suggests comparable electron-attracting tendencies despite structural differences (Dong et al. 2022). Chemical potential (μ) was less negative for compound **4** (−4.080 vs. −4.293 eV), indicating a reduced tendency for electron escape (Dong et al. 2022).

The electrophilicity index (ω) was higher for compound **3** (3.875 eV) compared with compound **4** (3.179 eV), indicating that compound **3** has a greater capacity to accept electrons from nucleophilic sites (Parr et al. 1999; Pal and Chattaraj 2023). This contradicts the finding that compound **4** exhibits

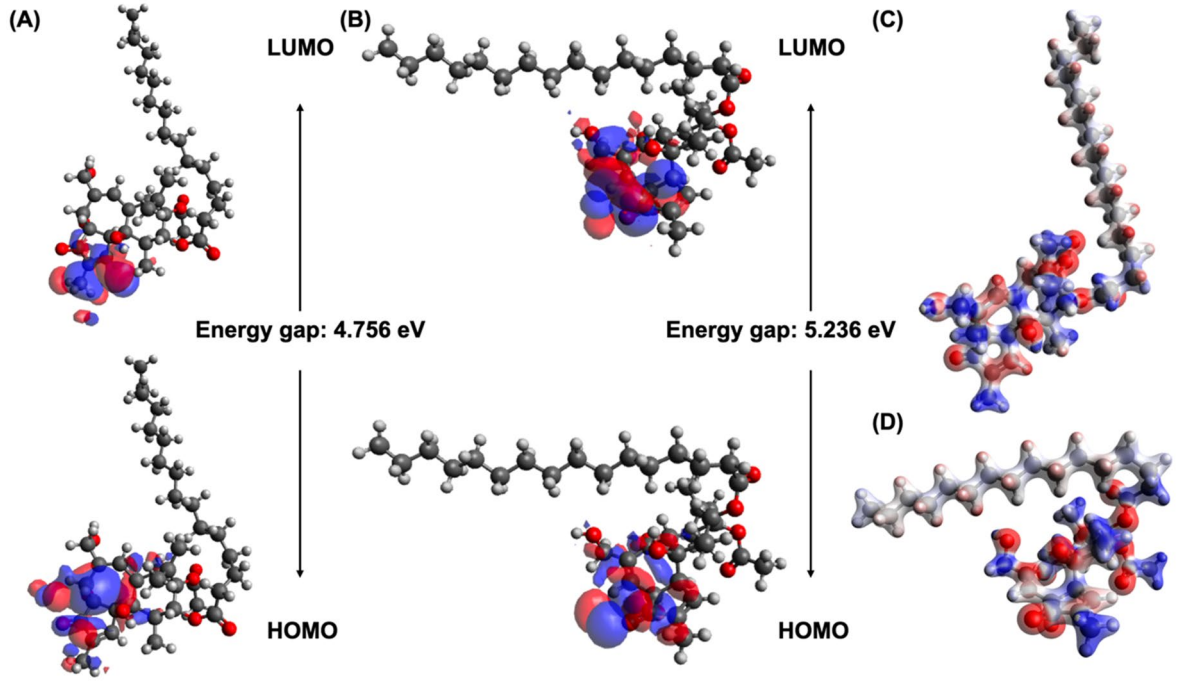

Figure 2. The electronic properties of compounds **3** and **4**. (A) The frontier molecular orbital of compound **3**; (B) The frontier molecular orbital of compound **4**; (C) Molecular electrostatic potential map for compound **3**; (D) Molecular electrostatic potential map for compound **4**.

superior cytotoxicity, despite being less electrophilic. In some cases, a high electrophilicity index may be correlated with superior biological activity for certain compounds; however, this may not be the case for antiproliferative and cytotoxic activities (Selvaraju et al. 2019; Marinescu et al. 2020). Thus, we used multiple indicators in the DFT calculation to justify our findings.

Network pharmacology

Because of the superior antiproliferative activity of diterpenes **3** and **4**, we used network pharmacology to elucidate their mechanisms of action against colorectal cancer. Data mining from the two diterpenes revealed a diverse target profile that strongly supports their potential as anticancer drugs. A total of 103 potential protein targets were identified, with kinases representing 46.7%, followed by oxidoreductases (13.3%), and voltage-gated ion channels (13.3%) (Figure 3(A)). This kinase pattern is consistent with established mechanisms in colorectal cancer pathogenesis, in which dysregulation of MAPK, PI3K/AKT, and protein kinase C drives proliferation, survival, and metastasis (Stefani et al. 2021; Song et al. 2024). A Venn diagram (Figure 3(B)) revealed that both compounds interact with 43 shared targets (3.8% of 1,133 colon cancer-associated genes), which were selected for protein–protein interaction (PPI) network, KEGG pathway enrichment, and molecular function analyses.

Table 3. Global chemical reactivity descriptors of the diterpenes.

	Compounds	
Descriptors	**3**	**4**
HOMO	−6.671	−6.698
LUMO	−1.915	−1.462
E_gap	4.756	5.236
I	6.671	6.698
A	1.915	1.462
η	2.378	2.618
S	0.210	0.191
X	4.293	4.080
μ	−4.293	−4.080
ω	3.875	3.179

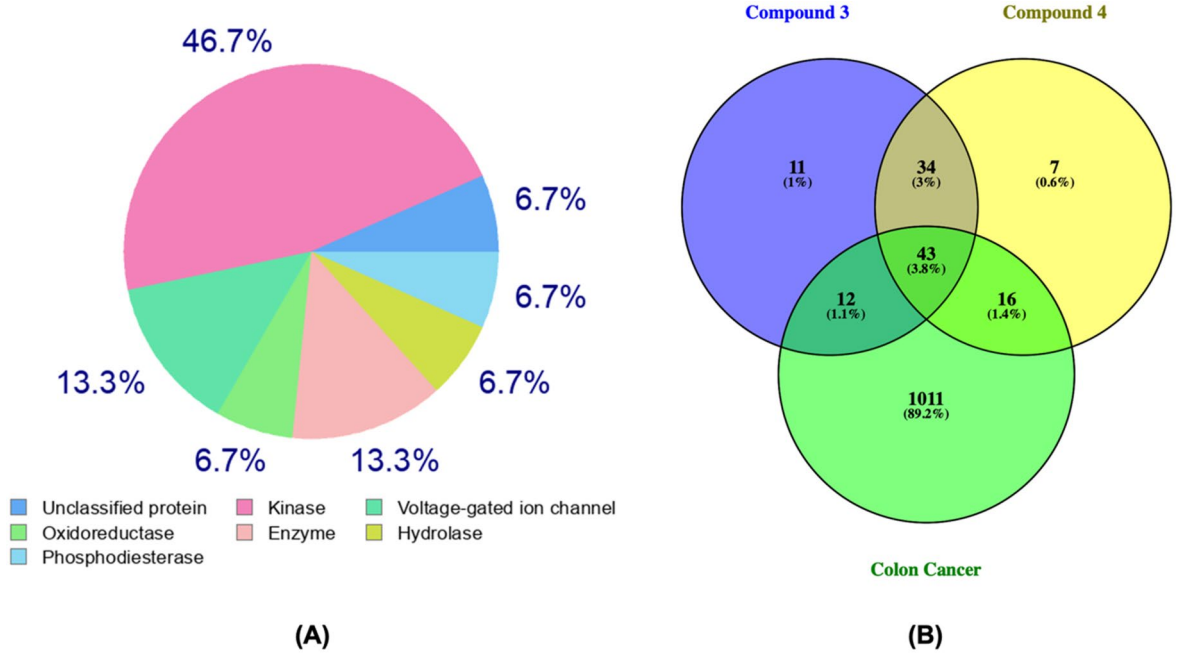

Figure 3. Target identification of compounds **3** and **4**. (A) Top 15 target-based classification; (B) Crossmatch of compounds **3** and **4** with Colon cancer-related genes.

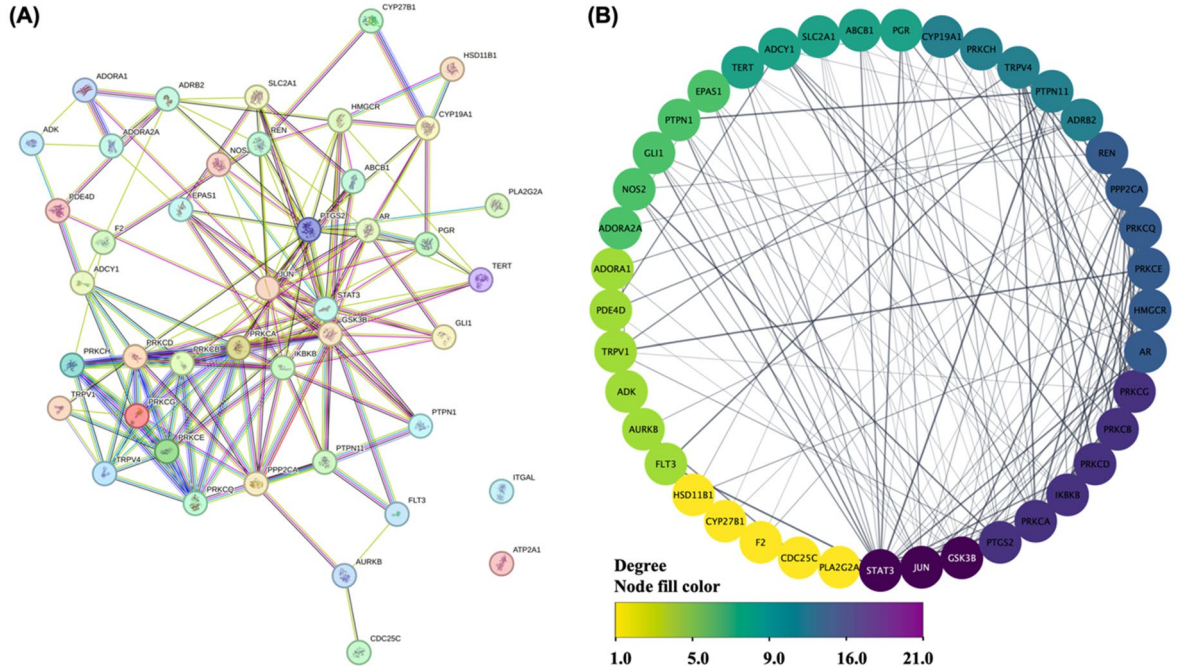

Figure 4. Protein–protein interactions of 48 genes (A) and their topological analysis with a color shift from dark purple to yellow, indicating a shift from high to low degree of connectivity (B).

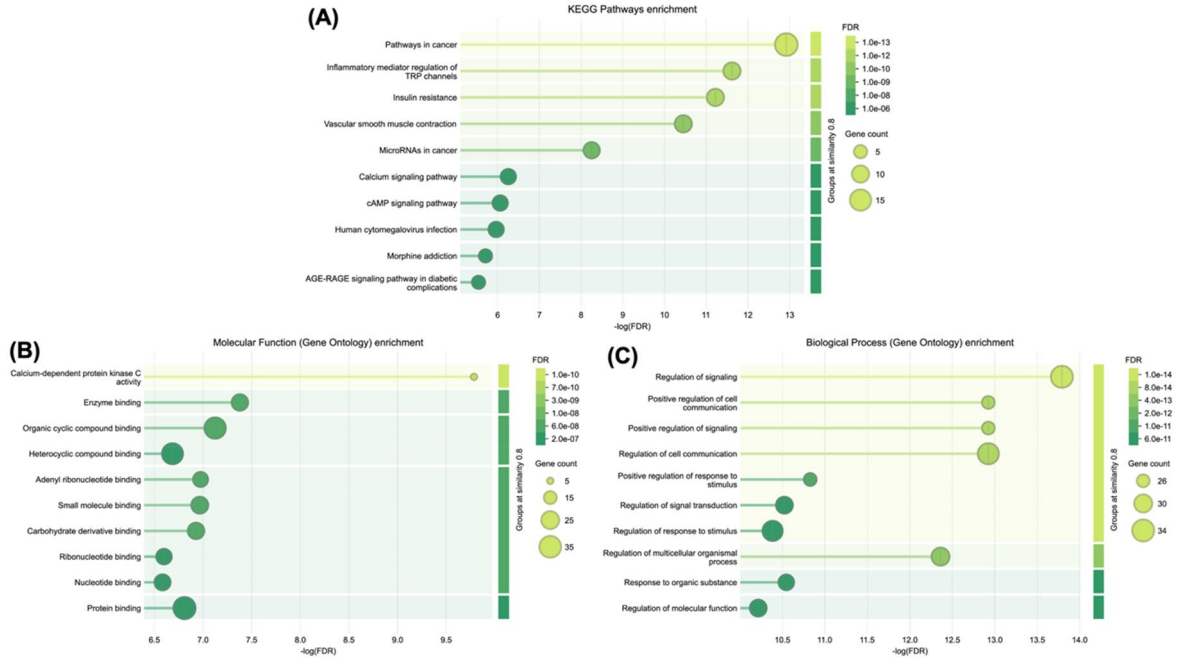

Figure 5. Enrichment analysis. (A) KEGG pathways; (B) Gene ontology molecular function; (C) Gene ontology biological process.

A PPI network analysis was done to understand their biological connection and relevance. The PPI network revealed densely connected hubs around STAT3, JUN, PRKCA, and GSK3β. Moreover, a topological analysis (Figure 4(B)) identified these proteins as master regulators with the highest connectivity degrees (18-21 interactions), whereas the peripheral targets showed lower connectivity (1–5 interactions). This hierarchical organization suggests that diterpenes not only affect central regulatory hubs, but also peripheral specialized functions.

KEGG pathway enrichment analysis (Figure 5(A)) revealed 'Pathways in cancer' as the most significantly enriched category (~15 genes), which directly validates the disease-specific relevance. Enrichment of insulin resistance and inflammatory mediator regulation of TRP channels correlated with established colorectal cancer risk factors, whereas calcium and cAMP signaling pathways represented fundamental second messenger systems that regulate proliferation and apoptosis. Molecular function analysis (Figure 5(B)) revealed calcium-dependent protein kinase C activity as the most enriched function, which correlates with kinase predominance in target classification. Moreover, biological process enrichment (Figure 5(C)) revealed 'regulation of signaling' as the top category, which indicates that these compounds may fundamentally alter cancer cell signal processing and environmental responses (Lv and Li 2019; Yang et al. 2019).

The integrated compound–pathway–gene network based on the analyses indicated that both diterpenes connect to all major pathways through the hub genes, STAT3, JUN, GSK3β, and PRKCA (Figure 6). This multi-target, multi-pathway engagement pattern is characteristic of natural products, which offer advantages over single-target therapeutics, as they may exert more robust anticancer effects, while limiting the development of resistance (Gomez-Cadena et al. n.d.; Muhammad et al. 2022; Soumya et al. 2024).

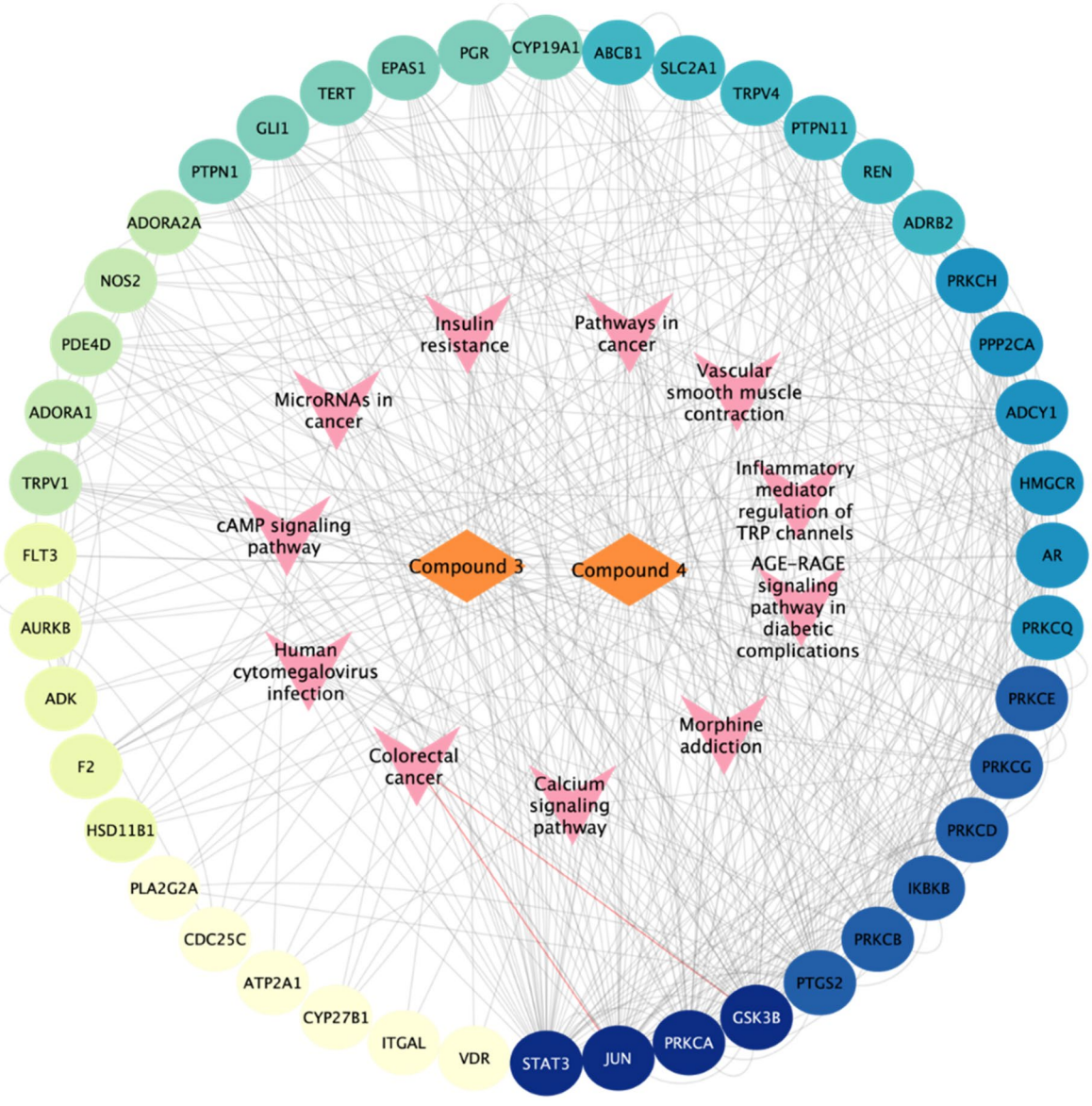

Figure 6. Compound–pathway–gene network.

Molecular docking

To validate the predicted interactions and evaluate the structure-activity relationships between compounds **3** and **4**, molecular docking studies were conducted against the four hub target genes identified from network pharmacology.

Molecular docking analysis revealed distinct binding preferences that correlated with compound cytotoxicity (Table 4). Compound **4** showed superior binding to the kinases, PRKCA (−5.10 kcal/mol) and GSK3β (−4.16 kcal/mol), whereas compound **3** exhibited preferential binding to the transcription factors, STAT3 (−4.96 kcal/mol) and JUN (−4.67 kcal/mol). PRKCA emerged as the target with the strongest affinity for both diterpenes, whereas compound **4** showed the most favorable binding energy among all compound-target pairs.

In the PRKCA binding site (Figure 7), compound **4** demonstrated extensive π-alkyl interactions (Ala 366, Leu 345, Val 420, Tyr 419, and Met 470), conventional hydrogen bonding (Asn 468), and a unique sulfur interaction (Met 470), while avoiding unfavorable acceptor–acceptor interactions with Glu 387, which was observed for compound **3**. This optimized binding mode likely explains the superior binding energy (−5.10 vs −4.99 kcal/mol) of compound **4** and correlates with its 3.5-fold enhanced cytotoxicity.

For GSK3β (Figure 8), compound **4** showed enhanced hydrogen bonding (Lys 188, Asn 244) along with extensive hydrophobic interactions, which explains its 0.43 kcal/mol superior binding compared with compound **3**. Meanwhile, for the STAT3 and JUN binding sites (Supplementary), compound **3** established more extensive interaction networks, particularly for JUN, in which it formed multiple π-alkyl interactions (Ile 70, 124; Leu 206; Met 146, 149; Ala 91; Val 78, 196) and conventional hydrogen bonds (Asp 150).

The differential target engagement profiles directly correlated with the observed biological activities. Compound **4,** with a kinase-focused mechanism (PRKCA and GSK3β), showed superior cytotoxicity (IC_{50} 3.58–6.06 μM) compared with compound **3** (IC_{50} 12.37–30.36 μM), with a transcription factor preference (STAT3/JUN). This may be the result of the rapid effects of kinase inhibition on cell signaling and proliferation pathways, producing immediate responses that are evident within a standard 72-hour cytotoxicity assay (Cousins et al. 2018; Martelli et al. 2022). In contrast, the compound **3** pattern likely required extended time for transcriptional reprogramming to manifest as measurable cytotoxicity, coupled with cellular compensatory mechanisms and transcriptional network redundancy. This may partially overcome the inhibition of individual transcription factors (Chen and Koehler 2020; Brennan et al. 2022).

Pharmacokinetics and toxicological predictions

One of the challenges in drug discovery and development research is the scarcity of pharmacokinetic data (Pei et al. 2023; Paliwal et al. 2024). Therefore, we also established the pharmacokinetic data for the diterpenes using pkCSM, a web-based server to assess their drug development potential (Pires et al. 2015).

The pkCSM analysis revealed favorable pharmacokinetic profiles for both diterpenes (Table 5). Water solubility values (−4.283 and −4.142 log mol/L) indicated adequate aqueous solubility, which supports oral bioavailability. Compound **3** demonstrated superior intestinal permeability (Caco-2: 0.752 vs 0.29 log Papp), which suggests higher absorption (79.4% vs 74.6%) and a lower required dose compared with compound **4**. Both compounds showed minimal skin permeability (−2.535 and −2.674 log Kp), thus indicating favorable safety margins against topical exposure.

Distribution analysis revealed that both diterpenes function as P-glycoprotein substrates and inhibitors, which indicates a potential for drug-drug interactions. Extensive plasma protein binding (fraction unbound: 0 and 0.007) suggested reduced free drug concentrations, although protein-bound reservoirs

Table 4. The docking score of compounds **3** and **4** against core targets identified from network pharmacology.

	Binding free energy (kcal/mol)			
Compound	STAT3	JUN	PRKCA	GSK3β
3	−4.96	−4.67	−4.99	−3.73
4	−4.80	−4.30	−5.10	−4.16
Doxorubicin	−5.80	−6.40	−5.48	−4.79

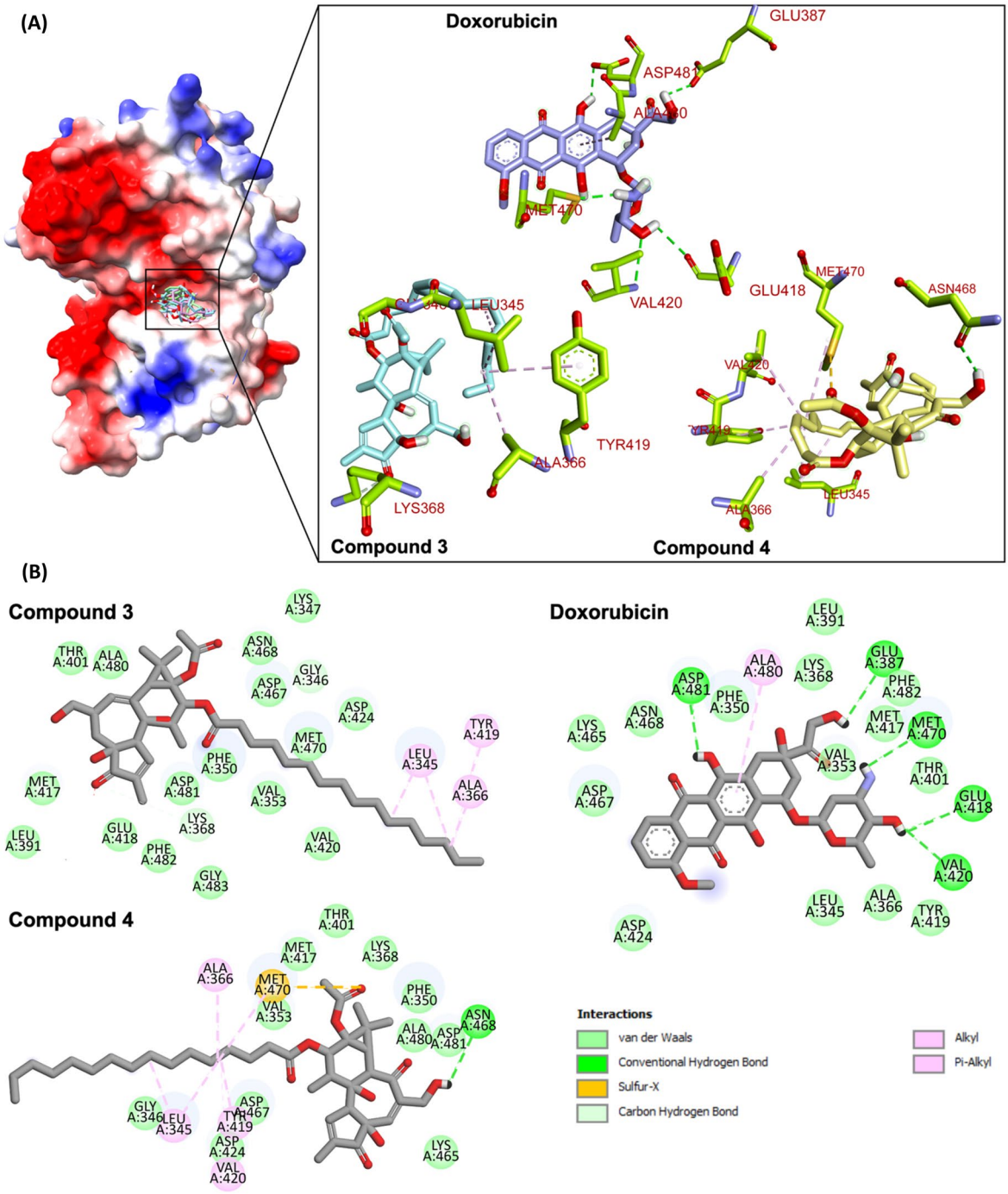

Figure 7. Molecular interactions of compound 3 and 4 with amino acid residues of PRKCA binding site. (A) Compounds bound to PRKCA active site and the highlight of their 3D interactions. (B) a clear tow-dimensional visualization of the molecular interactions.

may extend the duration of action. CNS penetration was limited (BBB: −1.55 and −1.649 log BB), which minimizes the risk of neurological adverse reactions.

Metabolic profiling identified both compounds as CYP3A4 substrates, without interactions with other major CYP450 isoforms (CYP2D6, CYP1A2, CYP2C19, and CYP2C9). Thus, co-administration with CYP3A4 inhibitors (ketoconazole, clarithromycin) or inducers (rifampicin, carbamazepine) could significantly alter therapeutic efficacy. The negative AMES prediction indicates safety margins as well as acute and chronic toxicity prediction, which indicates that the diterpenes (**3** and **4**) are suitable for therapeutic development.

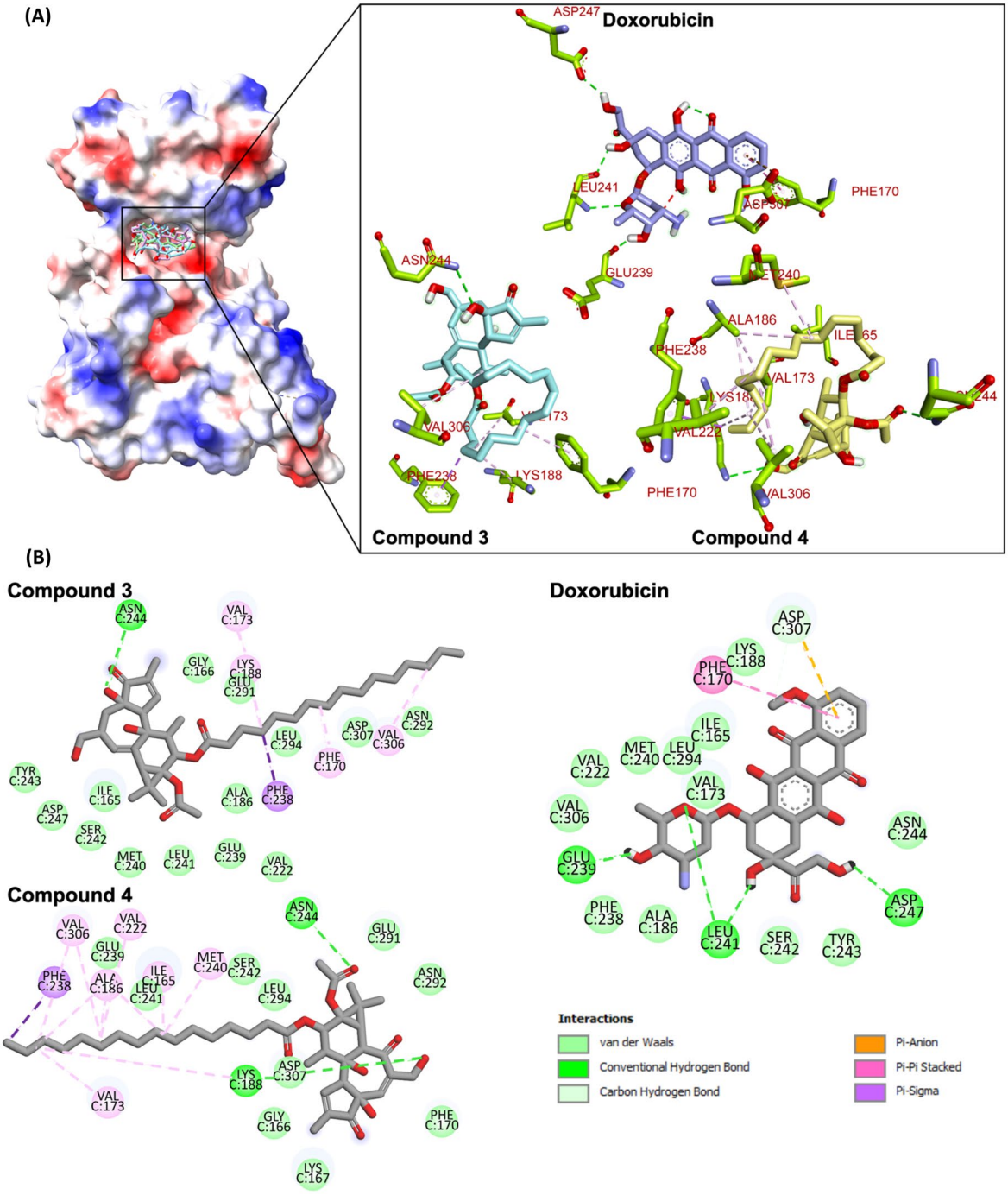

Figure 8. Molecular interactions of compound **3** and **4** with amino acid residues of GSK3β binding site. (A) Compounds bound to GSK3β active site and the highlight of their 3D interactions. (B) a clear tow-dimensional visualization of the molecular interactions.

Discussion

In the present study, six compounds were isolated, which included two diterpenoids, 12-*O*-palmitoyl-phorbol-13-acetate (**3**), 12-*O*-palmitoyl-7-oxo-5-ene-phorbol-13-acetate (**4**), and four triterpenoids, 7β-hydroxysitosterol (**1**), 7α-hydroxysitosterol (**2**), cerevisterol (**5**), and β-sitosterol-3-*O*-β-D-glucoside (**6**). All compounds were isolated from *H. giganteus* for the first time. This phytochemical study provides new information for the largely unexplored *Homalanthus* genus, in which only 5 of 23 species have been chemically characterized (Wirasisya and Hohmann 2023).

Table 5. Predictive pharmacokinetics and toxicological profile of compounds **3** and **4**.

Parameters	Compounds		Unit
	3	**4**	
Water solubility	−4.283	−4.142	Numeric (log mol/L)
Caco2 permeability	0.752	0.29	Numeric (log Papp in 10^{-6} cm/s)
Intestinal absorption (human)	79.388	74.55	Numeric (% Absorbed)
Skin Permeability	−2.535	−2.674	Numeric (log Kp)
P-glycoprotein substrate	Yes	Yes	Categorical (Yes/No)
P-glycoprotein I inhibitor	Yes	Yes	Categorical (Yes/No)
P-glycoprotein II inhibitor	Yes	Yes	Categorical (Yes/No)
VDss (human)	−0.555	−0.392	Numeric (log L/kg)
Fraction unbound (human)	0	0.007	Numeric (Fu)
BBB permeability	−1.55	−1.649	Numeric (log BB)
CNS permeability	−2.607	−2.78	Numeric (log PS)
CYP2D6 substrate	No	No	Categorical (Yes/No)
CYP3A4 substrate	Yes	Yes	Categorical (Yes/No)
CYP1A2 inhibitior	No	No	Categorical (Yes/No)
CYP2C19 inhibitior	No	No	Categorical (Yes/No)
CYP2C9 inhibitior	No	No	Categorical (Yes/No)
CYP2D6 inhibitior	No	No	Categorical (Yes/No)
CYP3A4 inhibitior	No	No	Categorical (Yes/No)
Total Clearance	0.708	0.672	Numeric (log ml/min/kg)
Renal OCT2 substrate	No	No	Categorical (Yes/No)
AMES toxicity	No	No	Categorical (Yes/No)
Max. tolerated dose (human)	−0.934	−0.868	Numeric (log mg/kg/day)
hERG I inhibitor	No	No	Categorical (Yes/No)
hERG II inhibitor	Yes	Yes	Categorical (Yes/No)
Oral Rat Acute Toxicity (LD50)	5.195	5.06	Numeric (mol/kg)
Oral Rat Chronic Toxicity (LOAEL)	2.933	3.249	Numeric (log mg/kg_bw/day)
Hepatotoxicity	No	No	Categorical (Yes/No)
Skin Sensitization	No	No	Categorical (Yes/No)
T. pyriformis toxicity	0.285	0.285	Numeric (log ug/L)
Minnow toxicity	−1.176	−0.795	Numeric (log mM)

Among the isolated compounds, the 3.8-fold superior antiproliferative activity of 7β-hydroxysitosterol (**1**) versus its 7α-epimer (**2**) against Colo 205 cells demonstrated the importance of C-7 stereochemistry in oxysterol cytotoxicity. This preference for the β-configuration was established, in which compound **1** induced apoptosis in the Caco-2 cell line through sequential caspase-9/3 activation and mitochondrial membrane permeabilization (Roussi et al. 2007, 2005). The inverted selectivity of β-sitosterol-3-*O*-glucoside (**6**) against Colo 320 cells (RF = 0.45) was also interesting. Based on our results, compound **6** may exert drug resistance-modifying activity (Szakács et al. 2014; Efferth et al. 2020).

The two diterpenes (**3** and **4**) exhibited the highest antiproliferative activity, greatly exceeding that of the sterols (**1**, **2**, **6**) against Colo 205 cells. This is consistent with numerous previous studies showing that diterpenes from Euphorbiaceae plants are generally more effective against cancer compared with triterpenes (Kemboi et al. 2021; Jiménez-González et al. 2023; Shakeri et al. 2024).

The most interesting result was the 3.5-fold IC_{50} difference against COLO 205 cells between the structurally similar diterpenes (**3** and **4**). This difference in activity illustrates a nuanced structure-activity relationship, in which greater calculated chemical reactivity does not yield superior biological potency. Our DFT results indicated that compound **3** contains a smaller HOMO-LUMO gap (4.756 eV) and a higher electrophilicity index (3.875 eV), indicating that it is more reactive; however, it was less active compared with compound **4**.

This paradox may occur because compound **3** has a $\Delta^{6(7)}$ double bond that could trigger oxidative rearrangements during isolation and under biological conditions. Thus, the higher reactivity of compound **3** may be the result of chemical instability rather than selective target engagement, which likely leads to off-target reactions and weaker pharmacological potency (Selvaraju et al. 2019; Marinescu et al. 2020).

In contrast, compound **4** has a larger energy gap (5.236 eV), higher chemical hardness (2.618 eV), and lower electrophilicity (3.179 eV), which indicates that it is more chemically stable. The C-7 ketone and $\Delta^{5(6)}$ double bond pulls electrons away from the rest of the molecule and stabilizes its structure. This is evident in the MEP maps, which show specific patterns of charge distribution around these

groups (Figure 8(B)). This stability causes the molecule to interact with specific protein targets, rather than reacting randomly with various molecules that may alter its activity (Abbaz et al. 2018).

To determine how diterpenes suppress colon cancer, we conducted network pharmacology and molecular docking, which revealed 103 potential targets with remarkable kinase enrichment (46.7%). In addition, 43 genes correlated with the diterpenes directly validated the mechanistic basis for diterpene cytotoxicity as a kinase regulator (Yoshida et al. 2001; Shen et al. 2010; Kostenko et al. 2011). Molecular docking revealed different targeting strategies between diterpenes **3** and **4**, which may explain their differences in activity. Compound **4** preferentially binds to the kinases, PRKCA (−5.10 kcal/mol) and GSK3β (−4.16 kcal/mol), and correlates with superior cytotoxicity (IC_{50} 3.58–6.06 µM, RF = 1.69). This may occur because kinase inhibition affects cell signaling (Watson et al. 2020). PRKCA mediates signal transduction downstream of growth factor receptors (Stephenson and Higgins 2023), whereas GSK3β regulates Wnt signaling, which also promotes colon cancer cell survival (Cousins et al. 2018). Simultaneous disruption of these genes is observable within a 72-hour MTT assay.

The preference of compound **3** for transcription factors STAT3 (−4.96 kcal/mol) and JUN (−4.67 kcal/mol) explains its weaker activity (IC_{50} 12.37-30.36 µM, RF = 2.45). Transcriptional reprogramming requires extended timeframes for altered gene expression to accumulate sufficiently to trigger cell cycle arrest or apoptosis (Chen and Koehler 2020). In addition, cells exhibit transcriptional network redundancy, in which multiple transcription factors compensate for single-target inhibition, which may limit the impact of STAT3 or JUN blockade alone (Schaefer et al. 1995; Zhang et al. 1999).

The molecular basis for the superior binding of compound **4** to PRKCA lies in its unique sulfur interaction with Met 470 and hydrogen bonding with Asn 468, while avoiding an unfavorable acceptor–acceptor clash with Glu 387, which was observed for compound **3**. DFT analysis supported this difference through the C-7 ketone, establishing distinct electrostatic environments that enable stronger interactions with the binding pocket architecture of PRKCA. This represents a clear case in which computational chemical properties can be translated into macromolecular and biological activity (Sayed et al. 2023; Azam et al. 2025).

Although the molecular docking and DFT calculations suggest promising drug development potential, pkCSM predictions revealed that both diterpenes possess adequate oral bioavailability with intestinal absorption reaching 74–79%. Based on our calculation, limited CNS penetration occurs (BBB −1.55 to −1.649 log BB), which reduces the risk of brain-related adverse effects. Thus, diterpenes **3** and **4** are likely suitable for colorectal cancer treatment. However, it is important to note that all pharmacokinetic data discussed above are based on computational predictions and should be experimentally validated. This is particularly important considering the established tumor-promoting effects of tigliane esters through PKC activation (Ohigashi et al. 1983; Vasas and Hohmann 2014).

Conclusions

This study represents the first detailed phytochemical investigation of *H. giganteus*, in which six compounds were successfully isolated and characterized, including two tigliane diterpenes (**3** and **4**), three sterols (**1**, **2,** and **5**), and one sterol glycoside (**6**). These were all isolated for the first time from this species. Among the isolated compounds, 12-*O*-palmitoyl-7-oxo-5-ene-phorbol-13-acetate (**4**) was identified as the most promising. Compound **4**, a diterpene, is chemically stable, targets kinases, shows promising activity with IC_{50} values of 3.58 ± 0.37 µM (Colo 205) and 6.06 ± 1.70 µM (Colo 320), and has predicted oral drug-like properties. These findings suggest that *H. giganteus* is a promising source of lead compounds for colorectal cancer therapy. Nevertheless, network pharmacology and molecular docking are computational prediction methods; therefore, experimental validation of the predicted targets and comprehensive *in vitro* and *in vivo* toxicological assessments are required before further development.

Acknowledgments

The authors thank Dr. Róbert Berkecz (Department of Pharmaceutical Analysis, University of Szeged) for the mass spectrometry measurements, and RotaChrome Technologies PLC (Kecskemét, Hungary) for performing the CPC experiment.

Authorship contribution statement

CRediT: **Dyke Gita Wirasisya**: Conceptualization, Data curation, Investigation, Writing – original draft; **Annamária Kincses**: Data curation, Investigation, Validation; **Arif Setiawansyah**: Investigation, Visualization; **Anita Barta**: Data curation, Investigation; **Fang-Rong Chang**: Resources, Supervision; **Judit Hohmann**: Conceptualization, Funding acquisition, Supervision, Validation, Writing – review & editing.

Disclosure statement

No potential conflict of interest was reported by the authors.

Funding

This work was supported by the Ministry of Innovation and Technology of Hungary (grant number TKP2021-EGA-32). The authors acknowledge a bilateral mobility grant from the Hungarian Academy of Sciences (NKM2024-16/2024) and the National Science and Technology Council, Taiwan (NSTC-HAS 111-2927-I-037 501).

Data availability statement

All data supporting the findings of this study are included within the main text of the article and its Supplementary Information files.

References

Abbaz T, Bendjeddou A, Villemin D. 2018. Molecular orbital studies (hardness, chemical potential, electro negativity and electrophilicity) of TTFs conjugated between 1, 3-dithiole. Int J Adv Res Sci Eng Technol. 5(2):5151–5161.

Abedizadeh R, Majidi F, Khorasani HR, Abedi H, Sabour D. 2024. Colorectal cancer: a comprehensive review of carcinogenesis, diagnosis, and novel strategies for classified treatments. Cancer Metastasis Rev. 43(2):729–753. https://doi.org/10.1007/s10555-023-10158-3

Abu-Izneid T et al. 2024. Density functional theory (DFT), molecular docking, and xanthine oxidase inhibitory studies of dinaphthodiospyrol S from *Diospyros kaki* L. Saudi Pharm J. 32(2):101936. https://doi.org/10.1016/j.jsps.2023.101936

Alves ALV, da Silva LS, Faleiros CA, Silva VAO, Reis RM. 2022. The role of ingenane diterpenes in cancer therapy: from bioactive secondary compounds to small molecules. Nat Prod Commun. 17(7):1934578X221105691. https://doi.org/10.1177/1934578X221105691

Appendino G, Gaeta S. 2024. Tigliane diterpenoids. In: Kinghorn, A.D., Falk, H., Gibbons, S., Asakawa, Y., Liu, J.-K., Dirsch, V.M. (Eds.), Tigliane diterpenoids. Springer Nature: Switzerland, p. 1–189. https://doi.org/10.1007/978-3-031-67180-7_1

Azam M et al. 2025. Profiling of antioxidant properties and identification of potential analgesic inhibitory activities of *Allophylus villosus* and *Mycetia sinensis* employing *in vivo*, *in vitro*, and computational techniques. J Ethnopharmacol. 336:118695. https://doi.org/10.1016/j.jep.2024.118695

Baloch IB, Baloch MK, Najam Us Saqib Q. 2005. Tumor-promoting diterpene esters from latex of Euphorbia cauducifolia L. Helv Chim Acta. 88(12):3145–3150. https://doi.org/10.1002/hlca.200590254

Barta A et al. 2025. Phenanthrene monomers and dimers from juncus tenuis with antiproliferative activity and synergistic effect with doxorubicin against human colon cancer cell lines. Int J Mol Sci. 26(16):7665. https://doi.org/10.3390/ijms26167665

Bourdy G, François C, Andary C, Boucard M. 1996. Maternity and medicinal plants in Vanuatu II. Pharmacological screening of five selected species. J Ethnopharmacol. 52(3):139–143. https://doi.org/10.1016/0378-8741(96)01404-3

Brennan A, Leech JT, Kad NM, Mason JM. 2022. An approach to derive functional peptide inhibitors of transcription factor activity. JACS Au. 2(4):996–1006. https://doi.org/10.1021/jacsau.2c00105

Casares R et al. 2022. Engineering the HOMO–LUMO gap of indeno[1,2-b]fluorene. J Mater Chem C. 10(32):11775–11782. https://doi.org/10.1039/D2TC02475F

Chaurasia N, Wichtl M. 1987. Sterols and steryl glycosides from urtica dioica. J Nat Prod. 50(5):881–885. https://doi.org/10.1021/np50053a018

Chen A, Koehler AN. 2020. Transcription factor inhibition: lessons learned and emerging targets. Trends Mol Med. 26(5):508–518. https://doi.org/10.1016/j.molmed.2020.01.004

Chicoye E, Powrie WD, Fennema O. 1968. Photoxidation of cholesterol in spray-dried egg yolk upon irradiation. J Food Sci. 33(6):581–587. https://doi.org/10.1111/j.1365-2621.1968.tb09078.x
Cousins EM et al. 2018. competitive kinase enrichment proteomics reveals that abemaciclib inhibits GSK3β and activates WNT signaling. Mol Cancer Res. 16(2):333–344. https://doi.org/10.1158/1541-7786.MCR-17-0468
Dong X, Oganov AR, Cui H, Zhou X-F, Wang H-T. 2022. Electronegativity and chemical hardness of elements under pressure. Proc Natl Acad Sci U S A. 119(10):e2117416119. https://doi.org/10.1073/pnas.2117416119
Efferth T et al. 2020. Collateral sensitivity of natural products in drug-resistant cancer cells. Biotechnol Adv. 38:107342. https://doi.org/10.1016/j.biotechadv.2019.01.009
Forgo P et al. 2011. Unusual tigliane diterpenes from *Euphorbia grandicornis*. J Nat Prod. 74(4):639–643. https://doi.org/10.1021/np100673s
Frankova A et al. 2021. *In vitro* antibacterial activity of extracts from Samoan medicinal plants and their effect on proliferation and migration of human fibroblasts. J Ethnopharmacol. 264:113220. https://doi.org/10.1016/j.jep.2020.113220
Gomez-Cadena A, Barreto A, Fiorentino S, Jandus C. n.d. Immune system activation by natural products and complex fractions: a network pharmacology approach in cancer treatment. Cell Stress. 4(7):154–166. https://doi.org/10.15698/cst2020.07.224
Gustafson KR et al. 1992. A nonpromoting phorbol from the Samoan medicinal plant Homalanthus nutans inhibits cell killing by HIV-1. J Med Chem. 35(11):1978–1986. https://doi.org/10.1021/jm00089a006
Hall MD, Handley MD, Gottesman MM. 2009. Is resistance useless? Multidrug resistance and collateral sensitivity. Trends Pharmacol Sci. 30(10):546–556. https://doi.org/10.1016/j.tips.2009.07.003
Hashem S et al. 2022. Targeting cancer signaling pathways by natural products: exploring promising anti-cancer agents. Biomed Pharmacother. 150:113054. https://doi.org/10.1016/j.biopha.2022.113054
Hirota M, Ohigashi H, Koshimizu K. 1979. Piscicidal constituents and related diterpene esters from *Aleurites fordii*. Agric Biol Chem. 43(12):2523–2529. https://doi.org/10.1080/00021369.1979.10863840
Hu R et al. 2021. Structurally diverse triterpenoids with cytotoxicity from Euphorbia hypericifolia. Fitoterapia. 151:104888. https://doi.org/10.1016/j.fitote.2021.104888
Jiménez-González V et al. 2023. Nature's green potential: anticancer properties of plants of the Euphorbiaceae Family. Cancers (Basel). 16(1):114. https://doi.org/10.3390/cancers16010114
Johnson HE, Banack SA, Cox PA. 2008. Variability in content of the anti-AIDS Drug Candidate Prostratin in Samoan populations of Homalanthus nutans. J Nat Prod. 71(12):2041–2044. https://doi.org/10.1021/np800295m
Kaya S, Putz MV. 2022. Atoms-in-molecules' faces of chemical hardness by conceptual density functional theory. Molecules. 27(24):8825. https://doi.org/10.3390/molecules27248825
Kemboi D, Peter X, Langat M, Tembu J. 2020. A review of the ethnomedicinal uses, biological activities, and triterpenoids of Euphorbia Species. Molecules. 25(17):4019. https://doi.org/10.3390/molecules25174019
Kemboi D, Siwe-Noundou X, Krause RWM, Langat MK, Tembu VJ. 2021. Euphorbia diterpenes: an update of isolation, structure, pharmacological activities and structure-activity relationship. Molecules. 26(16):5055. https://doi.org/10.3390/molecules26165055
Kostenko S, Khan MTH, Sylte I, Moens U. 2011. The diterpenoid alkaloid noroxoaconitine is a Mapkap kinase 5 (MK5/PRAK) inhibitor. Cell Mol Life Sci. 68(2):289–301. https://doi.org/10.1007/s00018-010-0452-1
Krstić G et al. 2025. Anti-HIV activity of tigliane derivatives from Euphorbia nicaeensis roots. Molecules. 30(7):1452. https://doi.org/10.3390/molecules30071452
Lv J, Li L. 2019. Hub genes and key pathway identification in colorectal cancer based on bioinformatic analysis. Biomed Res Int. 2019:1545680. https://doi.org/10.1155/2019/1545680
Ma X-M et al. 2023. New abietane and tigliane diterpenoids from the roots of Euphorbia fischeriana and their cytotoxic activities. J Asian Nat Prod Res. 25(6):519–527. https://doi.org/10.1080/10286020.2023.2197224
Marinescu M et al. 2020. Synthesis, density functional theory study and in vitro antimicrobial evaluation of new benzimidazole Mannich bases. BMC Chem. 14(1):45. https://doi.org/10.1186/s13065-020-00697-z
Martelli AM, Paganelli F, Evangelisti C, Chiarini F, McCubrey JA. 2022. Pathobiology and therapeutic relevance of GSK-3 in chronic hematological malignancies. Cells. 11(11):1812. https://doi.org/10.3390/cells11111812
Miar M, Shiroudi A, Pourshamsian K, Oliaey AR, Hatamjafari F. 2021. Theoretical investigations on the HOMO–LUMO gap and global reactivity descriptor studies, natural bond orbital, and nucleus-independent chemical shifts analyses of 3-phenylbenzo[d]thiazole-2(3H)-imine and its para-substituted derivatives: solvent and substituent effects. J Chem Res. 45(1-2):147–158. https://doi.org/10.1177/1747519820932091
Muhammad N et al. 2022. The role of natural products and their multitargeted approach to treat solid cancer. Cells. 11(14):2209. https://doi.org/10.3390/cells11142209
Naeem A et al. 2022. Natural products as anticancer agents: current status and future perspectives. Molecules. 27(23):8367. https://doi.org/10.3390/molecules27238367
Neese F. 2025. Software update: the ORCA Program System—Version 6.0. WIREs Comput Mol Sci. 15(2):e70019. https://doi.org/10.1002/wcms.70019
Newman DJ, Cragg GM. 2020. Natural products as sources of new drugs over the nearly four decades from 01/1981 to 09/2019. J Nat Prod. 83(3):770–803. https://doi.org/10.1021/acs.jnatprod.9b01285

Ohigashi H et al. 1983. Tigliane type diterpene-esters with epstein–barr virus-inducing activity from *Sapium sebiferum*. Agric Biol Chem. 47(7):1617–1622. https://doi.org/10.1080/00021369.1983.10865799
Otsuki K, Li W. 2023. Tigliane and daphnane diterpenoids from Thymelaeaceae family: chemistry, biological activity, and potential in drug discovery. J Nat Med. 77(4):625–643. https://doi.org/10.1007/s11418-023-01713-x
Pal R, Chattaraj PK. 2023. Electrophilicity index revisited. J Comput Chem. 44(3):278–297. https://doi.org/10.1002/jcc.26886
Paliwal A et al. 2024. Predictive modelling in pharmacokinetics: from in-silico simulations to personalized medicine. Expert Opin Drug Metab Toxicol. 20(4):181–195. https://doi.org/10.1080/17425255.2024.2330666
Parr RG, Szentpály L. v, Liu S. 1999. Electrophilicity index. J Am Chem Soc. 121(9):1922–1924. https://doi.org/10.1021/ja983494x
Pei Q et al. 2023. Breaking the barriers of data scarcity in drug-target affinity prediction. Brief Bioinform. 24(6):bbad386. https://doi.org/10.1093/bib/bbad386
Pei Y-H et al. 2012. Tigliane diterpene esters with IFN γ-inducing activity from the leaves of *Aleurites fordii*. Bioorg Med Chem Lett. 22(6):2318–2320. https://doi.org/10.1016/j.bmcl.2012.01.057
Peshin T, Kar HK. 2017. Isolation and characterization of β-sitosterol-3-O-β-D-glucoside from the extract of the flowers of Viola odorata. BJPR. 16(4):1–8. https://doi.org/10.9734/BJPR/2017/33160
Pires DEV, Blundell TL, Ascher DB. 2015. pkCSM: predicting small-molecule pharmacokinetic and toxicity properties using graph-based signatures. J Med Chem. 58(9):4066–4072. https://doi.org/10.1021/acs.jmedchem.5b00104
Radhi AH. 2020. HOMO-LUMO energies and geometrical structures effecton corrosion inhibition for organic compounds predict by DFT and PM3 methods. nq. 18(1):37–45. https://doi.org/10.14704/nq.2020.18.1.NQ20105
Roh EM et al. 2010. Structural implication in cytotoxic effects of sterols from Sellaginella tamariscina. Arch Pharm Res. 33(9):1347–1353. https://doi.org/10.1007/s12272-010-0908-8
Rong C, Wang B, Zhao D, Liu S. 2020. Information-theoretic approach in density functional theory and its recent applications to chemical problems. WIREs Comput Mol Sci. 10(4):e1461. https://doi.org/10.1002/wcms.1461
Roussi S et al. 2007. Mitochondrial perturbation, oxidative stress and lysosomal destabilization are involved in 7β-hydroxysitosterol and 7β-hydroxycholesterol triggered apoptosis in human colon cancer cells. Apoptosis. 12(1):87–96. https://doi.org/10.1007/s10495-006-0485-y
Roussi S et al. 2005. Different apoptotic mechanisms are involved in the antiproliferative effects of 7β-hydroxysitosterol and 7β-hydroxycholesterol in human colon cancer cells. Cell Death Differ. 12(2):128–135. https://doi.org/10.1038/sj.cdd.4401530
Sadaqa E et al. 2025. pH-sensitive niosomal nanoencapsulation of beta- caryophyllene and its novel pathway in triple negative breast cancer. Biointerface Res Appl Chem. 15:1–18. https://doi.org/10.33263/BRIAC154.047
Sánchez-Hoyos F et al. 2024. Biological activity of the Euphorbiaceae and Moraceae families of medicinal plants present in the Northern Coast of Colombia: worldwide overview and their therapeutic potential. Braz J Develop. 10(6):e70775–e70775. https://doi.org/10.34117/bjdv10n6-060
Sayed HM et al. 2023. Phytochemical investigation, molecular docking studies and DFT calculations on the antidiabetic and cytotoxic activities of *Gmelina philippensis* CHAM. J Ethnopharmacol. 303:115938. https://doi.org/10.1016/j.jep.2022.115938
Schaefer TS, Sanders LK, Nathans D. 1995. Cooperative transcriptional activity of Jun and Stat3 beta, a short form of Stat3. Proc Natl Acad Sci U S A. 92(20):9097–9101. https://doi.org/10.1073/pnas.92.20.9097
Selvaraju K et al. 2019. Cytotoxic unsaturated electrophilic compounds commonly target the ubiquitin proteasome system. Sci Rep. 9(1):9841. https://doi.org/10.1038/s41598-019-46168-x
Shaik BB, Katari NK, Jonnalagadda SB. 2022. Role of natural products in developing novel anticancer agents: a perspective. Chem Biodivers. 19(11):e202200535. https://doi.org/10.1002/cbdv.202200535
Shakeri A et al. 2024. Diverse diterpenoids and a triterpenoid from *Euphorbia spinidens* Bornm. ex Prokh. Fitoterapia. 173:105838. https://doi.org/10.1016/j.fitote.2024.105838
Shen T et al. 2010. Cafestol, a Coffee-specific diterpene, is a novel extracellular signal-regulated kinase inhibitor with AP-1-targeted inhibition of prostaglandin E2 production in lipopolysaccharide-activated macrophages. Biol Pharm Bull. 33(1):128–132. https://doi.org/10.1248/bpb.33.128
Siegel RL, Wagle NS, Cercek A, Smith RA, Jemal A. 2023. Colorectal cancer statistics, 2023. CA Cancer J Clin. 73(3):233–254. https://doi.org/10.3322/caac.21772
Sintya E, Wijayanti N, Noraeni A. 2019. The effect of Homalanthus populneus (Giesel.) pax. extract in expression of T-cell receptor: inhibition study of HIV infection. Int J App Pharm. 11:134–137. https://doi.org/10.22159/ijap.2019.v11s5.T0106
Song Y, Chen M, Wei Y, Ma X, Shi H. 2024. Signaling pathways in colorectal cancer: implications for the target therapies. Mol Biomed. 5(1):21. https://doi.org/10.1186/s43556-024-00178-y
Soumya SJ et al. 2024. Multi-target and natural product-based multi-drug approach for anti-VEGF resistance in glioblastoma. Explor Drug Sci. 2:567–582. https://doi.org/10.37349/eds.2024.00062
Stefani C et al. 2021. Growth factors, PI3K/AKT/mTOR and MAPK signaling pathways in colorectal cancer pathogenesis: where are we now? Int J Mol Sci. 22(19):10260. https://doi.org/10.3390/ijms221910260

Stephenson EH, Higgins JMG. 2023. Pharmacological approaches to understanding protein kinase signaling networks. Front Pharmacol. 14:1310135. https://doi.org/10.3389/fphar.2023.1310135
Susanti G, Aldi Y, Handayani D, Ismed F, Setiawansyah A. 2025. Uncovering the pharmacological mechanism of ficus elastica as anti-hyperlipidemia candidate: LC-HRMS, network pharmacology, in vitro and in vivo studies. J Multidiscip Appl Nat Sci. 5(1):332–351. https://doi.org/10.47352/jmans.2774-3047.249
Susianti S et al. 2024. Integrating the network pharmacology and molecular docking confirmed with in vitro toxicity to reveal potential mechanism of non–polar fraction of cyperus rotundus linn as anti-cancer candidate. J Multidiscip Appl Nat Sci. 5(1):56–73. https://doi.org/10.47352/jmans.2774-3047.228
Szakács G et al. 2014. Targeting the achilles heel of multidrug-resistant cancer by exploiting the fitness cost of resistance. Chem Rev. 114(11):5753–5774. https://doi.org/10.1021/cr4006236
Trott O, Olson AJ. 2010. AutoDock Vina: improving the speed and accuracy of docking with a new scoring function, efficient optimization and multithreading. J Comput Chem. 31(2):455–461. https://doi.org/10.1002/jcc.21334
Vasas A, Hohmann J. 2014. Euphorbia diterpenes: isolation, structure, biological activity, and synthesis (2008–2012). Chem Rev. 114(17):8579–8612. https://doi.org/10.1021/cr400541j
Vela F, Ezzanad A, Hunter AC, Macías-Sánchez AJ, Hernández-Galán R. 2022. Pharmacological potential of lathyrane-type diterpenoids from phytochemical sources. Pharmaceuticals (Basel). 15(7):780. https://doi.org/10.3390/ph15070780
Vogg G et al. 1999. Tumor promoting diterpenes from *Euphorbia leuconeura* L. Phytochemistry. 51(2):289–295. https://doi.org/10.1016/S0031-9422(99)00016-3
Wang GQ, Gu JF, Gao YC, Dai YJ. 2016. Daucosterol inhibits colon cancer growth by inducing apoptosis, inhibiting cell migration and invasion and targeting caspase signalling pathway. Bangladesh J Pharmacol. 11(2):395–401. https://doi.org/10.3329/bjp.v11i2.25754
Wang Q, Shen X, Chen G, Du J. 2022. Drug resistance in colorectal cancer: from mechanism to clinic. Cancers (Basel). 14(12):2928. https://doi.org/10.3390/cancers14122928
Watson NA et al. 2020. Kinase inhibition profiles as a tool to identify kinases for specific phosphorylation sites. Nat Commun. 11(1):1684. https://doi.org/10.1038/s41467-020-15428-0
WHO. 2023. Colorectal cancer [WWW Document]. URL https://www.who.int/news-room/fact-sheets/detail/colorectal-cancer. (accessed 10.13.25).
Wirasisya DG, Hohmann J. 2023. An overview of the traditional use, phytochemistry, and biological activity of the genus Homalanthus. Fitoterapia. 166:105466. https://doi.org/10.1016/j.fitote.2023.105466
Wirasisya DG et al. 2023. Indonesian Euphorbiaceae: ethnobotanical Survey, In Vitro Antibacterial, Antitumour Screening and Phytochemical Analysis of Euphorbia atoto. Plants (Basel). 12(22):3836. https://doi.org/10.3390/plants12223836
Wu Q-C et al. 2009. 13C-NMR data of three important diterpenes isolated from Euphorbia species. Molecules. 14(11):4454–4475. https://doi.org/10.3390/molecules14114454
Yang Q et al. 2019. Pathway enrichment analysis approach based on topological structure and updated annotation of pathway. Brief Bioinform. 20(1):168–177. https://doi.org/10.1093/bib/bbx091
Yoshida M et al. 2001. Antitumor action of the PKC activator gnidimacrin through cdk2 inhibition. Int J Cancer. 94(3):348–352. https://doi.org/10.1002/ijc.1476
Zhang X, Wrzeszczynska MH, Horvath CM, Darnell JE. 1999. Interacting regions in Stat3 and c-Jun that participate in cooperative transcriptional activation. Mol Cell Biol. 19(10):7138–7146. https://doi.org/10.1128/mcb.19.10.7138
Zhang X-L, Wang L, Li F, Yu K, Wang M-K. 2013. Cytotoxic phorbol esters of *Croton tiglium*. J Nat Prod. 76(5):858–864. https://doi.org/10.1021/np300832n
Zhao J et al. 2010. Antimicrobial metabolites from the endophytic fungus Pichia guilliermondii isolated from Paris polyphylla var. yunnanensis. Molecules. 15(11):7961–7970. https://doi.org/10.3390/molecules15117961
Zhou M et al. 2025. Ingenane diterpenoids from Euphorbia peplus as potential new CHK1 inhibitors that sensitize cancer cells to chemotherapy. J Nat Prod. 88(3):688–705. https://doi.org/10.1021/acs.jnatprod.4c01343